Dyes and Pigments 120 (2015) 175–183

Contents lists available at ScienceDirect

Dyes and Pigments

journal homepage: www.elsevier.com/locate/dyepig

Self-assembly of a series of thiocyanate complexes with high two-photon absorbing active in near-IR range and bioimaging applications

Dandan Li, Qiong Zhang, Xuchun Wang, Shengli Li, Hongping Zhou, Jieying Wu, Yupeng Tian*

Department of Chemistry, Key Laboratory of Functional Inorganic Materials Chemistry of Anhui Province, Anhui University, Hefei 230039, PR China

ARTICLE INFO

Article history:
Received 2 January 2015
Received in revised form
14 March 2015
Accepted 17 March 2015
Available online 16 April 2015

Keywords:
Two-photon absorption
2 PA cross-sections
Near-infrared
Hetero-metal
Structure–property
Cell imaging

ABSTRACT

A series of novel complexes bearing high fluorescence quantum yields and showing the peak two-photon absorption (2 PA) cross-sections in the near-infrared region, **$Zn(SCN)_2L_2$ (1)**, **$[Cd(SCN)_2L_2]_n$ (2)**, **$Co(SCN)_2L_4$ (3)**, **$Ni(SCN)_2L_4$ (4)**, **$[CdHgL_2(SCN)_4]_n$ (5)** and **$[MnHg(SCN)_4L_2]_n$ (6)**, containing functional chromophore (**L** = (E)-(4-diethyl anilinostyryl)pyridine), were synthesized in high yields. Crystal structures of all the complexes were confirmed. Hetero-metal complexes (**5**, **6**: L:M = 1:1) present much higher two-photon absorption (2 PA) cross-sections (σ) in comparison with those of the homo-metal complexes (L:M = 4:1 in **3** and **4**, L:M = 2:1 in **1** and **2**) and the free ligand (**L**) which may due to the fact that the hetero-metal complexes have more bridged anions (SCN^-), conjugated subunits –$[Hg(SCN)_2M]$– and –$[Hg_2(SCN)_4M_2]$–. In addition, the results revealed that 2 PA response was much enhanced for the **$Zn(SCN)_2L_2$** and two-photon fluorescence cell imaging experiment proved its potential application.

1. Introduction

The research for functionalized materials with large molecular 2 PA cross sections (σ) has mushroomed because of their potential applications in two-photon excitation fluorescence microscopy [1–8], microfabrication [9,10], laser up-conversion [11–15], optical power limiting [16–18], three-dimensional (3D) fluorescence imaging [19–21], optical data storage [22–25], photodynamic therapy [26,27], two-photon fluorescent probe, and so on. Among these applications, bioimaging as two-photon fluorescence probes in living cells has recently been received much attention [28–30] due to the fact that among various conventional bio-imaging techniques, two-photon excitation microscopy is a highly sensitive and noninvasive tool particularly for living cell and tissue imaging. Since the 2 PA process is quadratic intensity dependent, the excitation in a two-photon excitation microscope is focused to a small volume in the focal plane where only in this volume there is sufficient laser intensity to generate appreciable excitation. The low photon flux outside the volume gives a negligible amount of fluorescence signal. As a result, the two-photon excitation process offers optical sectioning (depth discrimination) capability and higher spatial resolution. The confined excitation can greatly reduce the photobleaching and photodamage of the specimen during bioimaging. Most biological samples are relatively transparent to near-infrared light which shows less scattering and thus the use of the low-energy infrared excitation source can improve the penetration depth in tissues and cells allowing deeper tissue imaging. Furthermore, a high signal-to-noise ratio (SNR) can be achieved as the excitation and emission wavelengths are widely separated. To realize these applications, many strategies have been reported for the design of various two-photon absorbing materials [4,31–33], Much of the impetus for this technological exploration was provided by the synthesis of new dyes in the mid-1990s, which are much more efficient in direct 2 PA than those commercially available [34]. To facilitate the design and synthesis of new and stronger responsive two-photon absorbing materials, one available way to take advantage of the superior qualities of both inorganic and organic materials is to combine them in the same compound [35–48]. The introduction of ligated metal centers into an organic π-delocalizable framework may result in intense charge-transfer

* Corresponding author. Tel.: +86 551 5108151; fax: +86 551 5107342.
E-mail address: yptian@ahu.edu.cn (Y. Tian).

http://dx.doi.org/10.1016/j.dyepig.2015.03.039
0143-7208/

transitions and enhanced nonlinear optical response. In the nonlinear optical (NLO) material fields, thiocyanate complexes can been optimized for NLO properties by a polarizable π system, the hard nitrogen and the soft sulfur coordination, low-lying π* orbitals and the metal-to-ligand charge-transfer (MLCT) transition [49,50]. However, few endeavor has been devoted to investigation of the 2 PA effect of the thiocyanate complexes and different d electron configurations of transition metal complexes [51]. For pyridyl ligands, highly delocalized and easily polarizable system, can bind to a wide range of transition metal ions, and have large asymmetry in electronic distribution caused by intramolecular donor–acceptor charge transfer while they coordinate to metal ions [52]. In the case of the same organic ligand and anion SCN^-, how to choose metal ions to improve two-photon absorption cross section effectively is a scientific challenge, which can make contribution to the design of two-photon active complexes. These characters are crucial to design organic-inorganic hybrid materials with large 2 PA cross-section (σ).

Based on the consideration above, we have strategically designed and synthesized a series of novel thiocyanate complexes with high two-photon absorbing using $M(SCN)_2$ (M = Zn(II), Cd(II), Hg(II), Ni(II), Co(II), and Mn(II)) and pyridine ligand(**L**) (shown in Fig. 1). The structure–property relationships of these complexes have been systematically investigated. Considering the terminal sulfur atoms are relevant to biological systems [53,54], we singled out **$Zn(SCN)_2L_2$** (**1**) for biological imaging application research.

2. Experiments

2.1. General procedure

All chemicals and solvents were dried and purified by the standard methods. Elemental analysis was performed on a Perkin–Elmer 240C elemental analyzer. IR spectra were recorded with a Nicolet FTIR Nexus 870 instrument in the range 4000–400 cm^{-1} by using KBr pellets. ^1H NMR spectra were performed on a Bruker av 500 MHz Ultrashield spectrometer and are reported as parts per million (ppm) from TMS (δ). The linear absorption spectra were measured on a SPECORD S600 spectrophotometer. The single-photon emission fluorescence (SPEF) spectra measurements were performed using a Hitachi F-7000 fluorescence spectrophotometer. The two-photon emission fluorescence (TPEF) spectra were measured at femtosecond laser pulse and Ti: sapphire system (680–1080 nm, 80 MHz, 140 fs) as the light source. The excitation wavelengths for the complexes are 700–900 nm.

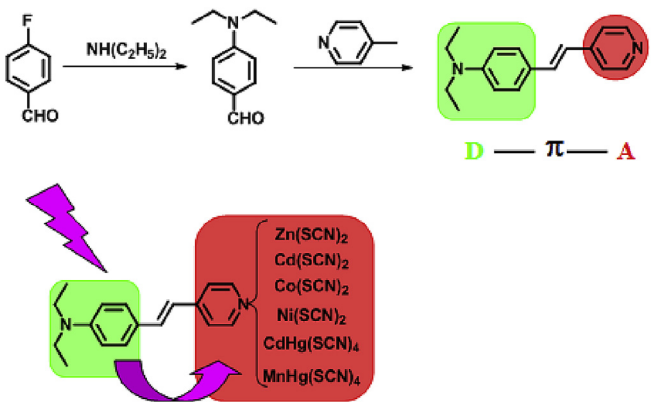

Fig. 1. Synthesis route of ligand.

2.2. Cell culture and incubation

HepG2 cells were seeded in 6 well plates at a density of 2 × 105 cells per well and grown for 96 h. For live cell imaging cell cultures were incubated with the chromophores (10% PBS: 90% cell media) at concentrations 40 μM and maintained at 37 °C in an atmosphere of 5% CO_2 and 95% air for incubation times ranging for 2 h. The cells were then washed with PBS (3 × 3 ml per well) and 3 ml of PBS was added to each well. The cells were imaged using confocal laser scanning microscopy and water immersion lenses.

2.3. Cell image

HepG2 cells were luminescently imaged on a Zeiss LSM 710 META upright confocal laser scanning microscope using magnification 40× and 100× water-dipping lenses for monolayer cultures. Image data acquisition and processing was performed using Zeiss LSM Image Browser, Zeiss LSM Image Expert and Image J.

2.4. Cytotoxicity assays in cells

To ascertain the cytotoxic effect of the compounds treatment over a 24 h period, the 5-dimethylthiazol-2-yl-2,5-diphenyl tetrazolium bromide (MTT) assay was performed. HepG2 cells were trypsinized and plated to ~70% confluence in 96-well plates 24 h before treatment. Prior to the compounds' treatment, the DMEM was removed and replaced with fresh DMEM, and aliquots of the compound stock solutions (500 μM DMSO) were added to obtain final concentrations of 1, 3, 5, 10, 20, 40, and 80 μM. The treated cells were incubated for 24 h at 37 °C and under 5% CO_2. Subsequently, the cells were treated with 5 mg/mL MTT (40 μL/well) and incubated for an additional 4 h (37 °C, 5% CO_2). Then, DMEM was removed, the formazan crystals were dissolved in DMSO (150 μL/well), and the absorbance at 490 nm was recorded. The cell viability (%) was calculated according to the following equation: cell viability % = OD_{490}(sample)/OD_{490}(control) × 100, where OD_{490}(sample) represents the optical density of the wells treated with various concentration of the compounds and OD_{490}(control) represents that of the wells treated with DMEM + 10% FCS. Three independent trials were conducted, and the averages and standard deviations are reported. The reported percent cell survival values are relative to untreated control cells.

2.5. Synthesis

The synthesis of the ligand and its complexes are shown in Supporting information.

2.6. Single-crystal structure analysis

Single-crystal measurements were carried out on a Bruker Smart 1000 CCD diffractometer equipped with a graphite crystal monochromator situated in the incident beam for data collection at room temperature. The determination of unit cell parameters and data collections were performed with M_o-K_α radiation (λ = 0.71073 Å). Unit cell dimensions were obtained with least-squares refinements, and all structures were solved by direct methods using SHELXL-97 [55]. The non-hydrogen atoms were located in successive difference Fourier syntheses. The final refinement was performed by full-matrix least-squares methods with anisotropic thermal parameters for non-hydrogen atoms on F^2. The hydrogen atoms were added theoretically and riding on the concerned atoms.

Crystallographic crystal data for complexes **1**–**6** are shown in Table S1. Selected bond lengths and bond angles are listed in

Tables S2 and S3. CCDC-621152 (for **1**) 256596 (for **2**), 256599 (for **3**), 621153 (for **4**), 256597 (for **5**) and 256600 (for **6**) contain the supplementary crystallographic data for this paper. These data can be obtained free of charge from The Cambridge Crystallographic Data Centre via www.ccdc.cam.ac.uk/data-request/cif.

3. Results and discussion

3.1. General characterization

IR spectra of the six complexes 1–6 showing strong or mediated bands at about 2970, 2100, 1585, 1520, and 1185 cm^{-1}, respectively, which are diagnostic peaks of coordinated L. The modes coordination of SCN^- in 1–6 can also be established by infrared spectroscopy that $\upsilon_{as}(NCS) \geq 2100\ cm^{-1}$ indicates a thiocyanate bridge with a 1,3-μ or 1,1,3-μ bridging mode [56]. The C≡N stretching vibrations of SCN^- at 2093, 2121 and 2123 cm^{-1} for 2, 5 and 6, respectively, suggest a bridging mode of SCN^- ligand, and the lower wave numbers (2079, 2061 and 2076 cm^{-1}, respectively) for 1, 3 and 4 exhibit a monodentate coordination mode, which are consistent with the results of X-ray single crystal diffraction analysis.

As depicted in the NMR spectra of free ligand and complexes, the chemical shift of complexes **1**–**6** exhibited slightly shift and the peak pattern changed as well (Figs. S1 and S2). The NMR spectra were collected at low concentrations, the above-mentioned phenomenon show that these complexes tend to preserve their original structural characters in themselves to some degree when dissolved in solution.

The UV–vis study of complexes 1–6 and L in DMF ($c = 5 \times 10^{-5}$ mol/L) exhibited strong absorption maxima (λ_{max}) in the range from 369 nm to 388 nm (Fig. S3), which ascribed to the π–π^* transition. The slight blue shift is observed for their absorption in DMF solution, due to opposite polar form in the ground and excited states [57].

3.2. Crystal structural determinations

3.2.1. Structures of the complexes

3.2.1.1. Four coordination $Zn(SCN)_2L_2$ (1). An ORTEP view of this complex is shown in Fig. 2, with the numbering scheme. The Zn(II) ion adopts a distorted tetrahedron coordination geometry and is coordinated by two nitrogen atoms from chromophores (**L**s) (the Zn–N(L) bond length (av) is 2.025 Å) and two from thiocyanate counterions with bond length of 1.940 Å. The average S–C and C–N distances (1.617 and 1.112 Å) in **1**, which are shorter than those (1.651 and 1.138 Å), in $[Cd(NCS)_3]_\infty$ [58], indicate a clear π-delocalization along the metal-thiocyanate branches. The shortening of bonds may result from some conjugation between two parts of the coordinated fragments, which also may due to the coplanar properties of the **L**s oriented in the same mode.

3.2.1.2. Six coordination: $Co(SCN)_2L_4$ (3) and $Ni(SCN)_2L_4$ (4). Each metal center in the complexes of this type adopts a pseudo-octahedral geometry with SCN^- ions occupying both axial positions and nitrogen donors from four chromophores (Ls) binding in the equatorial positions. The ORTEP plot of 3 is shown in Fig. 3 as an example (the structure of 4 is shown in the supporting information (Fig. S4)). The two linear SCN^- anions are nearly perpendicular to the equatorial plane with the N(SCN^-)-Co-N(L) angles being in the range from 89.70(2)° to 90.30(2)° (Table S3). The four equatorial Co–N bond lengths range from 2.203(6) to 2.230(5) Å are longer than those of the two axial Co–N bonds (2.049(6) Å and 2.049(6) Å) (Table S2). Similar bond lengths and angles have been observed in a Co(II) complex $[Co(bbbt)_2(NCS)_2]_n$ [59]. The average S–C and C–N distances of 1.610 and 1.150 Å in 3 and 1.642 and 1.130 Å in 4, respectively, the sums (2.760 Å for 3 and 2.772 Å for 4, respectively) of these two kind bond lengths are longer than those (2.729 Å) in 1, which indicate that 1 possesses a better π-delocalization along the metal-thiocyanate branches compared to 3 and 4. This π-delocalization in the molecule is highly important to improve the optical nonlinearity of the compound. Similarly, the bond lengths and angles around the nick(II) have normal values (Tables S2 and S3), which agree with those in Ni(II) complex $(L1)_4 \cdot Ni(SCN)_2$ [60].

3.2.2. Structures of coordination polymers

3.2.2.1. Homonuclear coordination polymer: $[Cd(SCN)_2L_2]_n$ (2). Crystallographic analyses show that each Cd atom in 2 is octahedrally coordinated with four nitrogen (from two chromophores and from two SCN^-, respectively) and two sulfur atoms, as illustrated in Fig. 4. The Cd atoms form an infinite linear chain of Cd atoms with

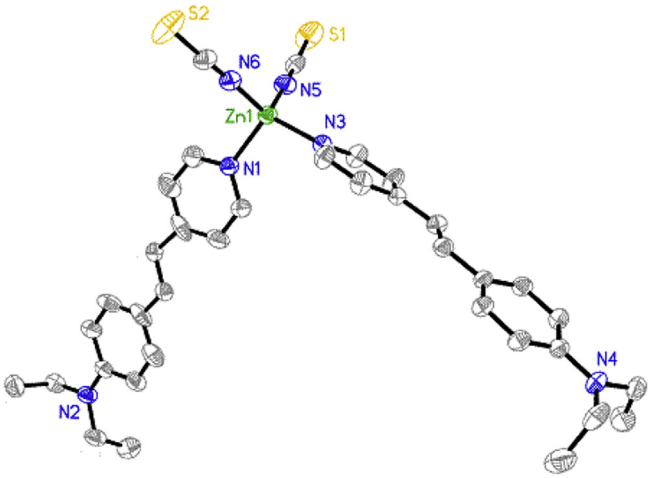

Fig. 2. ORTEP view of **1** with 50% thermal ellipsoids showing the atom-labeling scheme around the centric atoms. (Only the skeleton of the structure, hydrogen atoms were omitted for clarity).

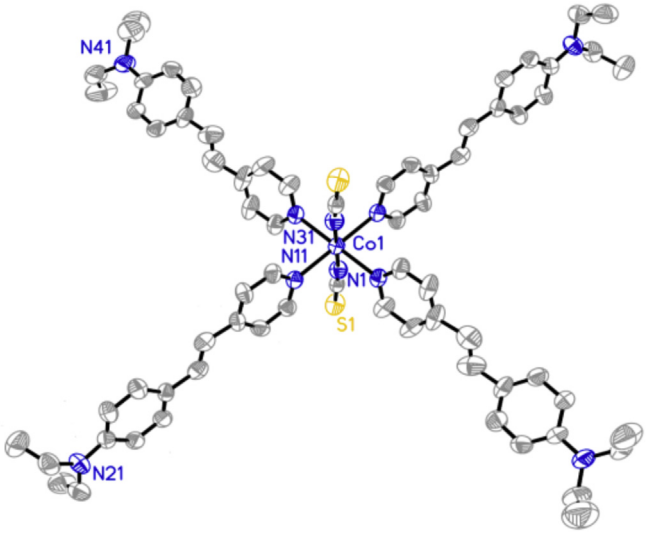

Fig. 3. ORTEP view of **3** with 50% thermal ellipsoids showing the atom-labeling scheme around the centric atoms. (Only the skeleton of the structure, hydrogen atoms were omitted for clarity).

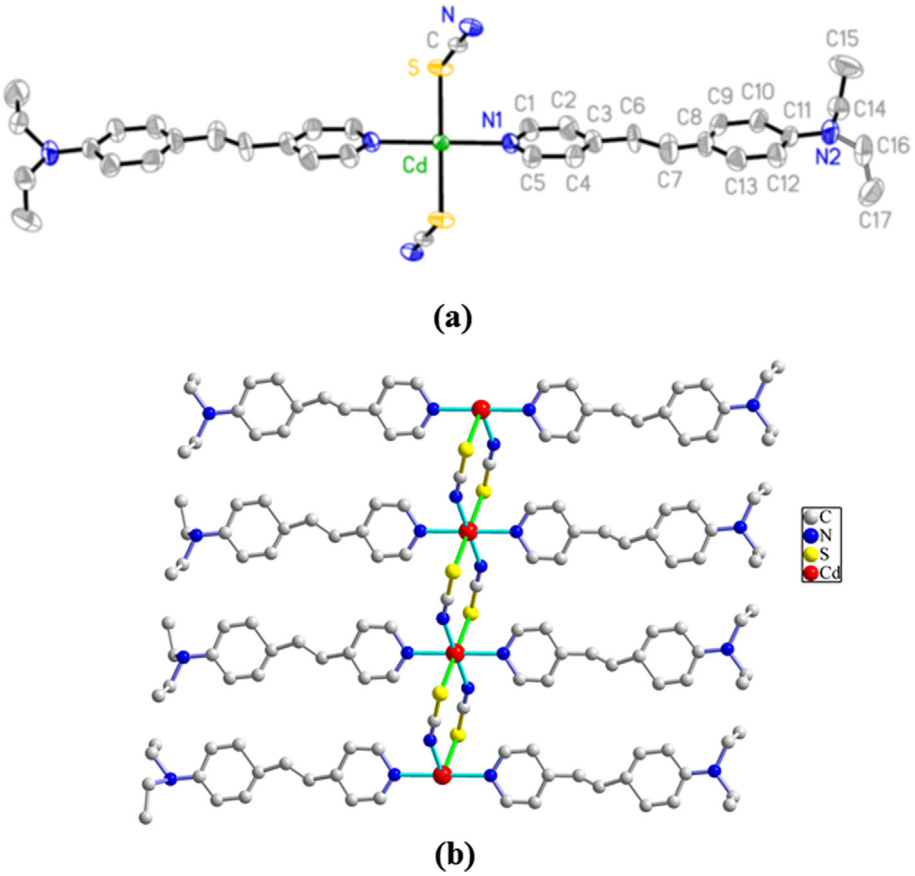

Fig. 4. ORTEP view of **2** [(a): unit and (b): packing] with 50% thermal ellipsoids showing the atom-labeling scheme around the centric atoms. (Only the skeleton of the structure, hydrogen atoms were omitted for clarity).

Cd•••Cd distance of 5.756 Å, which is slightly shorter than the value of 5.829 Å observed in $\{[Cd_3(deatrz)_4Cl_2(SCN)_4]_2H_2O\}_n$ [61], and Cd···Cd···Cd angle of 180°. The linear chains are parallel to one another and run along the crystallographic *a* axis. The two zig-zag-[S–C–N–Cd]$_\infty$- chains bundled around the central linear Cd···Cd chain, in which two thiocyanate ions bridge two Cd ions to form a rhombic $[Cd(SCN)_2Cd]$ eight-membered subunit gives the dimension of 2.744 × 4.958 Å (Fig. 4(b)). The chromophores are perpendicular to the two metal-thiocyanate chains, and like wings kinking at the Cd atoms. The adjacent stacks of Ls have their tails oriented in opposite directions, which leads to the most efficient crystal packing [62]. Due to larger size and the steric effect of the chromophore, the Cd–N(L) bond length (2.354(4) Å) is longer than Cd–N(SCN) bond length (2.289(4) Å). The average S–C and C–N distances (1.634 and 1.115 Å) in 2, which are longer than those in 1 but shorter than those in $[Cd(NCS)_3]_\infty$ [58], indicate a partial π-delocalization along the metal-thiocyanate chains.

3.2.2.2. Heteronuclear coordination polymer: $[CdHg(SCN)_4L_2]_n$ (5) and $[MnHg(SCN)_4L_2]_n$ (6). The results of single crystal X-ray diffraction analysis exhibit that both the complexes are structurally similar, the view of 5 is shown in Fig. 5 as an example (the crystal structure of 6 is shown in the Supporting Information). The basic unit of the same parent zig-zag motifs of 5 is made up of $-[Hg(SCN)_2Cd]-$ eight-member rhombohedral grids and $-[Hg_2(SCN)_4Cd_2]-$ sixteen-member rhombohedral grids P1 give the dimension of 6.259 × 5.981 Å and the diagonal distances of 6.898 × 10.115 Å, linked by SCN^- bridges to form two-dimensional zig-zag sheet. Here, the linearity of the bridging thiocyanate ions maintains S–C–N angles ranging from 177.7(6)° to 179.1(5)° (Table S3). The nature of bidentate thiocyanate ligand forms the layers and results in the formation of large 32-membered zig-zag grid P2. Moreover, the structural feature of the D–π–A ligand interpenetrating alternate multi-rings motif is rare. The thiocyate ligands chelate to centric cations forming large porous pseudo-aromatic rings, with the centric ions deviating from the planes of the grids, and this space plays a crucial role in determining the inclusion ability of the large chromophores. This structural feature of the large chromophore ligands interpenetrating alternate multi-rings motif can benefit excited-state charge redistribution and nonlinear optical properties.

3.3. Optical properties

3.3.1. Single-photon excited fluorescence (SPEF)

Single-photon excited fluorescence (SPEF) of the complexes **1**–**6** and **L** was measured in DMF dilute solutions (1×10^{-6} mol L^{-1}) by using Perkin–Elmer LS-55B fluorospectrometer (Fig. 6). When these complexes were excited at 380 nm, they underwent a one-photon strongly excited emission process, with the emission bands at wavelengths 471–475 nm and high fluorescence quantum yields (Φ_s) 40–87% (Table 1). Compared to their corresponding the free **L**, all complexes **1**–**6** show improved fluorescence quantum yields, may be due to strongly polarized D–π–A–M–A–π–D unit. The Φs values of hetero-metal complexes **5** and **6** are higher than those of homo-metal complexes **1**, **3**, **4**. This indicates that the fluorescence quantum yields can be tailored by the binding of metal ions for this chromophore.

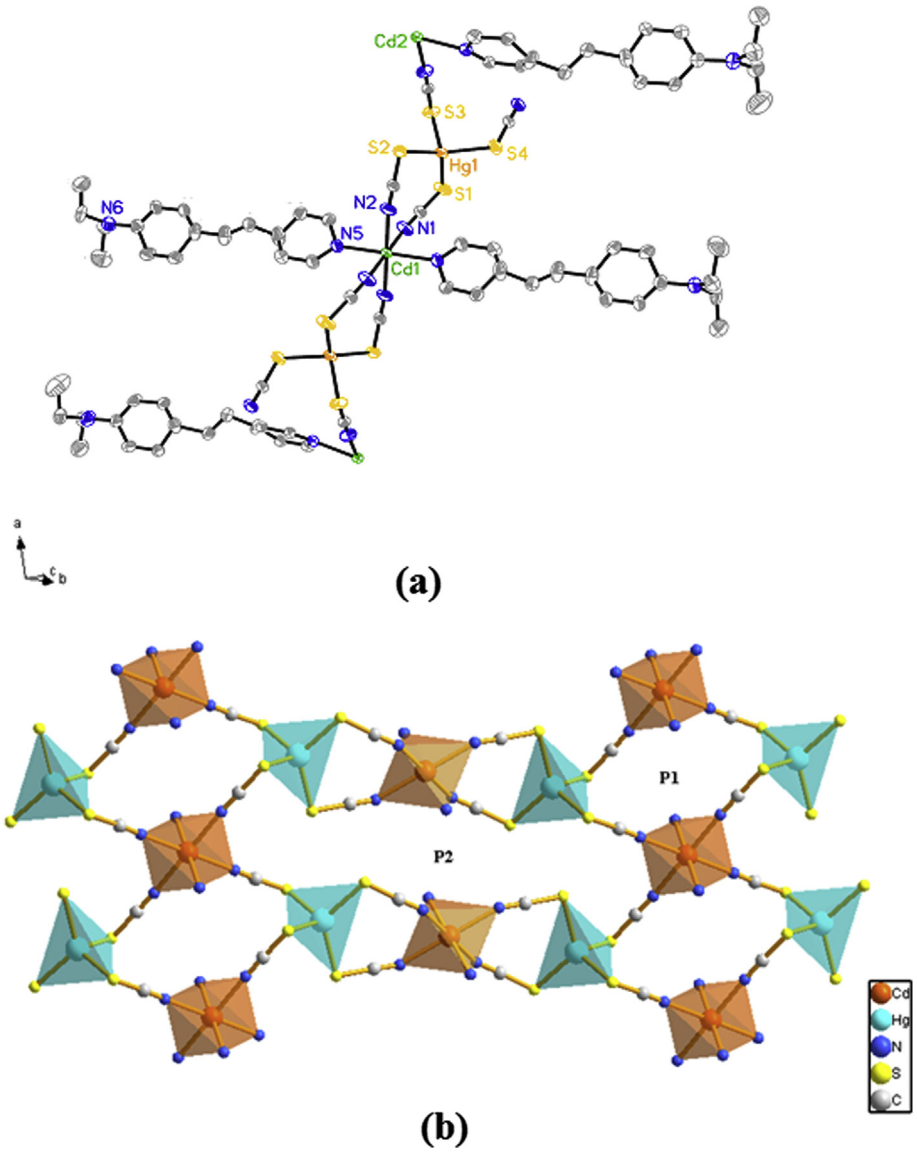

Fig. 5. View of **5** [(a): unit and (b): packing motifs]. (Only the skeleton of the structure, phenyl, ethyl groups and hydrogen atoms in **L** were omitted for clarity in packing motifs (b)).

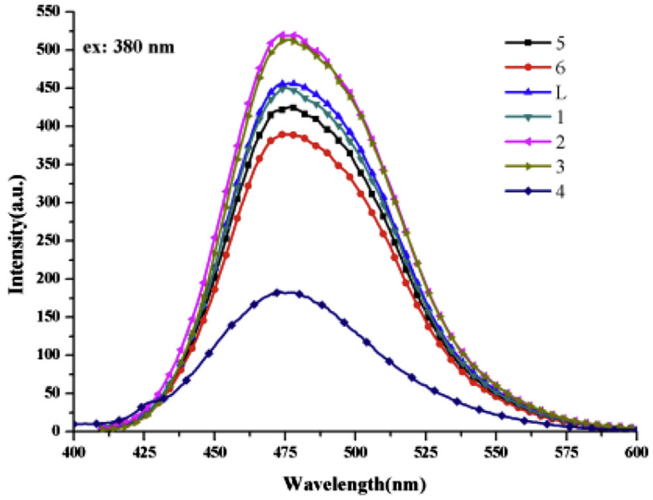

Fig. 6. Single-photon fluorescence spectra of the title complexes **1**–**6** and L in DMF (1×10^{-6} mol/L).

3.3.2. *Two-photon excited fluorescence spectra*

The two-photon excited fluorescence (TPEF) spectra of the six complexes 1–6 and free L in DMF ($C = 1.0 \times 10^{-4}$ mol L^{-1}) are shown in Fig. 7. (In all the case, the output intensity of two-photon excited fluorescence was squared dependent on the input laser, and the slope of the plot is about two in Fig. S6, thereby confirming the 2 PA process). The data were recorded in the excitation wavelength 760 nm. The Zn, Cd, Hg complexes have the stronger TPEF intensities compared to the Co(II), Ni(II) complexes. These d^{10} metal ions, having no ligand field stabilization energy, prefer coordination

Table 1
The spectra data of the title complexes **1**–**6** and **L** in DMF solution.

Compound	L	1	2	3	4	5	6
Φ_s (%)	39.3	74.2	66.5	50.0	59.6	60.4	78.7
σ^{max} GM[a]	302	1063	555	497	352	1128	1186
$\Phi\sigma^{max}$ [b]	118	789	370	249	211	283	935

[a] GM = 1×10^{-50} cm^4 s $photon^{-1}$ $molecule^{-1}$.
[b] Two-photon action cross section.

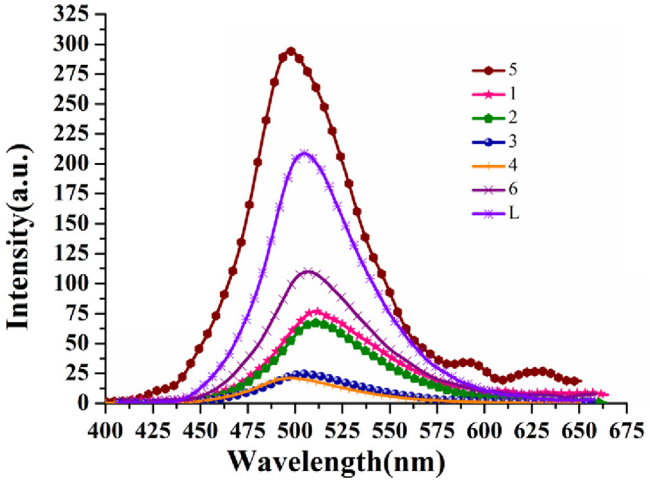

Fig. 7. Two-photon fluorescence spectra of the title complexes **1**–**6** and **L** in DMF (1×10^{-4} mol/L).

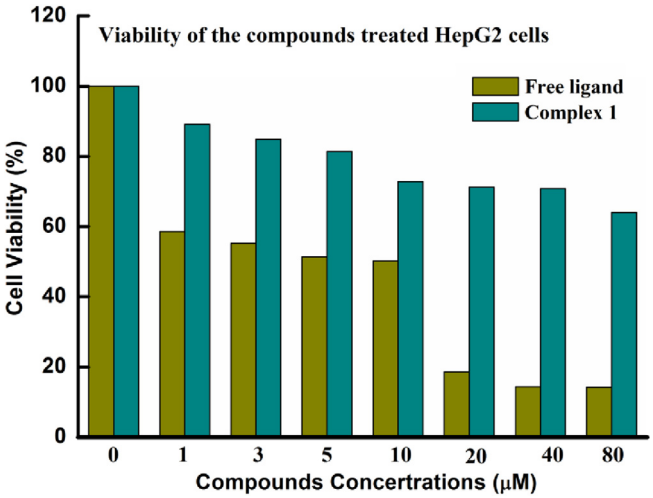

Fig. 9. MTT assay of HepG2 cells treated with free ligand **L** and complex **1** at different concentrations for 24 h.

geometry and are excellent 3D templates. The electron-acceptor character of Zn(II) or Cd(II) converts the chromophore and thiocyanate to more strongly polarized D–π–A units, which makes these complexes potential candidates for third-order nonlinear optical responses [63]. The TPEF peak positions of 1–6 show slight red-shift (3–12 nm) compared to the corresponding chromophore's peak position. However, the TPEF positions of the six complexes in DMF show clearly red-shift (about 30 nm) relative to their corresponding SPEF positions. This can be attributed to re-absorption effects, since all TPEF spectra were recorded in relative concentrated solutions while SPEF spectra were in dilute solutions in which the re-absorption is negligible.

3.3.3. *Two-photon absorption cross sections*

The 2 PA cross-sections (σ) in the 700–900 nm spectral range (Fig. 8) of 1–6 and free L were obtained by a comparison of the TPEF spectra of target molecules with fluorescein calibration standard (both at a concentration of 1×10^{-4} mol L^{-1}). The experimental errors are estimated to be ±10% from the variations of laser energies and sample concentrations. The 2 PA cross-section (σ) values were calculated by the following equation [57].

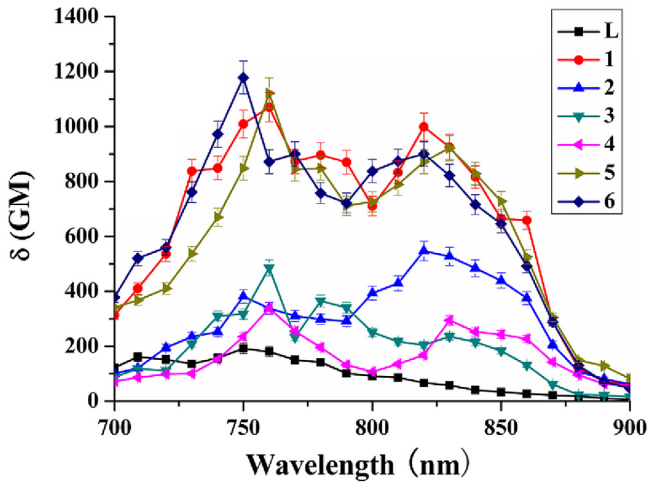

Fig. 8. Two-photon absorption spectra of **L, 1**–**6** in DMF (1×10^{-4} mol/L).

$$\sigma_S = \frac{S_S}{S_r}\frac{\Phi_r N_r n_r}{\Phi_S N_S n_S}\sigma_r$$

Here, S is the integrated area under the corrected emission, Φ is the quantum yield, N is the mol magnitude, n is the refractive index, subscripts s and r refer to the sample and reference solutions, respectively.

All of the complexes present two broad peaks in the 700–900 nm regions (Fig. 8), indicating the existence of two-photon absorption allowed states. (1) The incorporation of the chromophore (L) into the thiocyanate complexes induces a significant broadening and red-shift of the 2 PA spectra in the nearly whole red-NIR region, as illustrated in Fig. 8. This effect parallels the red-shift of both absorption and emission bands, that is, it correlates with the reduction of the electronic gap between ground and excited states [64]. This spectral character is particular importance for bioimaging and biological applications. (2) The σ values of 1–6 are clearly larger than that of the free chromophore L in the 700–900 nm region, due to 2 PA cross-section value correlating with intramolecular charge transfer to the π-bridge. The M(II) (M = Zn, Cd, Co, Ni, Hg and Mn) coordinated complexes have an extended π-bridge considering the π-electron contribution from the M(II) metal ions. And the metal ions favor the intramolecular charge transfer from the donors to the π-bridge. The enhancement of 2 PA properties of these complexes may be also attributed to the polarizable π-system of both the metal and the ligand, and low-lying π^* orbits of the SCN^- counter anion. (3) The σ values (Maximum: 1128–1186 GM) of the hetero-metal complexes (5, 6) are larger than those of homo-metal complexes (1–4). However, the density (L:M = 1:1) of chromophores in 5 and 6 is lower than that (L:M = 4:1 in 3 and 4, L:M = 2:1 in 1 and 2) of chromophore in homo-metal complexes. The results are seemingly not consistent with the theoretical explanation that 2 PA cross section would be enhanced with the increasing of chromophore density. We proposed that the hetero-metal complexes (5, 6) have more bridged anions (SCN^-), conjugated subunits $-[Hg(SCN)_2M]-$ and $-[Hg_2(SCN)_4M_2]-$, which give rise to strong metal-to-ligand charge-transfer (MLCT) excitations (or metal-mediated ligand $\pi \rightarrow \pi^*$ transitions), thereby, the values of their 2 PA cross-sections are greater than those of homo-nuclear metal ions complexes (1, 2, 3, 4). (4) The σ values of d^{10} metal ions (Zn, Cd) complexes (1, 2) are increased, compared to those of the d^8 ion (Ni(II)) and d^7 ion (Co(II)) complexes (3, 4), which proved that the d^{10} metal ions are more powerful modifications than other transition metal ions.

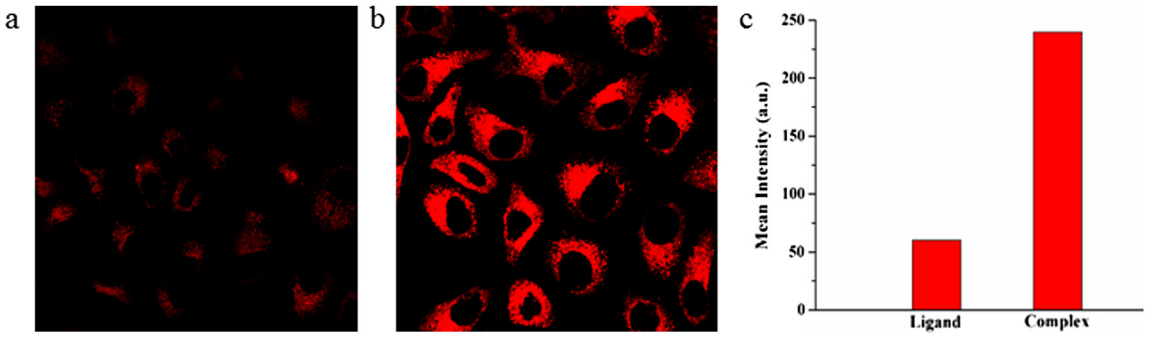

Fig. 10. (a) Two-photon image of HepG2 cells incubated with 20 μM **L** after 30 min of incubation, washed by PBS buffer. λ_{ex} = 760 nm (emission wavelength from 475 to 550 nm). (b) Two-photon image of HepG2 cells incubated with 20 μM complex **1** after 30 min of incubation, washed by PBS buffer. λ_{ex} = 760 nm (emission wavelength from 475 to 550 nm). (c) The two-photon luminescence intensity shown by **L** and complex **1.**

Maybe one suspects that the structures of the complexes will be destroyed in solution, while previous reports and our works exhibit that those compounds show themselves NLO effects in solution because they strongly tend to preserve their original structural characters in themselves to some degree [43,65–69]. Similarly, the molecules of **1**–**6** in this work may arrange as in the crystals, although aggregation chains may not be infinite as those in the solid crystals (Supporting information: The NMR spectra of free ligand and complexes). Furthermore, the 2 PA activities were performed in high concentration solutions. In order to further illustrate, we collected TPEF titration curves of **L** in the presence of different amounts of metal ion. In progress of titration, the concentration of **L** was constant but addition metal ion gradually into the system. As shown in Fig. S7, one can see that the two-photon fluorescence intensity varied with the amounts of metal ion. In addition, two-photon fluorescence intensity is the lowest for $Zn(SCN)_2$ titration and the strongest for $CdHg(SCN)_4$ titration, respectively, when achieving the best coordination model.

3.3.4. *Cytotoxicity tests (MTT assay)*

Considering the terminal sulfur atoms within the Zn(II) complex are relevant to biological systems, complex **1** was selected for MTT assay to ascertain the cytotoxic effect against HepG2 cells over a 24 h period. As a comparison, the MTT assay was performed to free ligand **L** at the same experimental conditions. Cytotoxicity is a potential side effect of dyes that must be controlled when dealing with living cells or tissues. Fig. 9 shows the cell viability for HepG2 cells treated with complex **1** and **L** at different concentrations for 24 h. The results clearly indicated that HepG2 cells incubated with

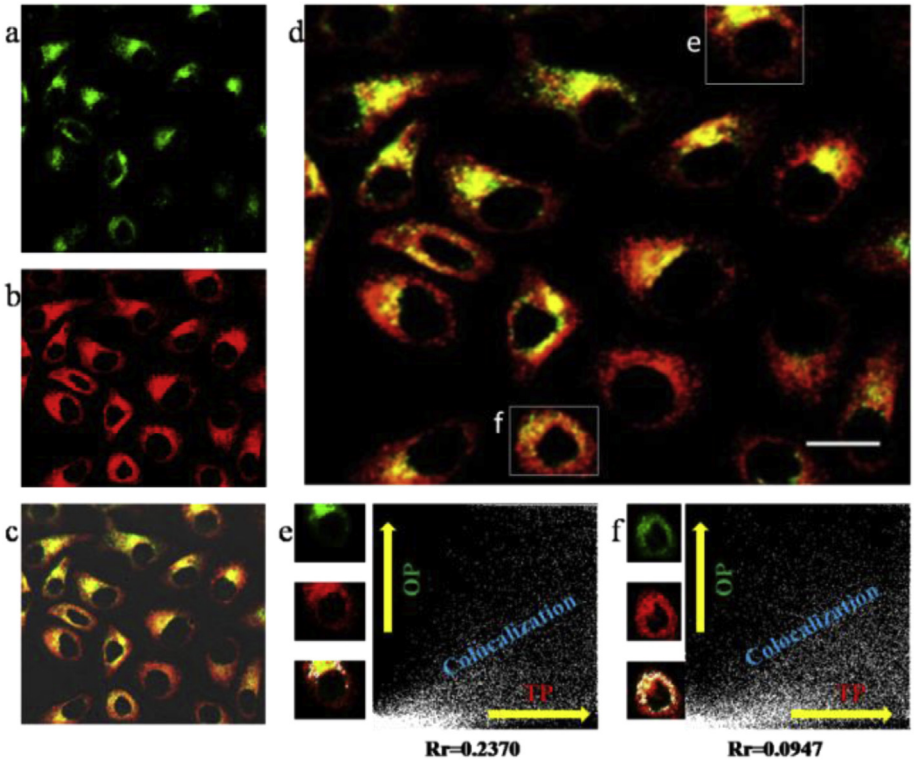

Fig. 11. (a) One-photon image of HepG2 cells incubated with 20 μM complex **1** after 20 min of incubation, washed by PBS buffer. λ_{ex} = 380 nm (emission wavelength from 450 to 500 nm). (b) Two-photon image of HepG2 cells incubated with 20 μM complex **1** after 30 min of incubation, washed by PBS buffer. λ_{ex} = 760 nm (emission wavelength from 475 to 550 nm). (c) differential interference contrast (DIC) image. (d) The overlay of (a) to (c). Scale bars represent 20 μm. (e) a high-level colocalization scatter plot between one-photon image and two-photon image. (f) a lower-level colocalization scatter plot between one-photon image and two-photon image.

concentration of 5 μM of complex **1** remained 82% viable, while 50% viable for free ligand **L**, after 24 h of feeding time, demonstrating the superior biocompatibility of complex **1**. Besides, it was found that high concentration only leads to a gradual decrease of viable cells as shown in Fig. 9. As a result, cytotoxicity tests definitely indicate that the low-micromolar concentrations of complex **1** have low toxic effects on living cells over a period of 24 h, and complex **1** is indeed has great potentials for further biological studies. It should be noted that the lower toxicity further proves that the complex tends to preserve its original structural characters in itself to some degree when dissolved in solution.

3.3.5. Bio-imaging application of complex 1

To evaluate the performance of complex **1** in living cells, one-photon and two-photon fluorescence microscopy (2PFM) imaging was performed and a cytotoxicity analysis was conducted. HepG2 cells were the testing candidates and were cultured and stained with complex **1**. As a comparison, autofluorescence images (Fig. S8) and images of cells incubated with the ligand **L** (Fig. S9) were performed at the same experimental conditions. A bright-field image of each cell was taken immediately prior to the 1PFM and 2PFM imaging. The 1PFM and 2PFM image and the merged image show that after 2 h incubation with HepG2 cells, the results showed that 1) The cells do not exhibit autofluorescence at this experimental condition; 2) Different from complex **1**, for the free ligand **L**, the cell apoptosis can be observed due to its high toxicity, and the 2 PE is much less bright than the 1 PE. Furthermore, using the same concentration, however, the two-photon luminescence intensity shown by **L** (mean intensity: 60.30) to drop approximately 1/4 times lower than complex **1** (mean intensity: 239.67) (Fig. 10). We also evaluated the colocalization profile between one-photon excitation channel and two-photon excitation channel from indicated single cell in Fig. 11(d)–(f) showed high-colocalization scatter plot and lower-colocalization scatter plot, respectively. The colocalization results demonstrated two-photon excitation signal dominated over one-photon signal, this might be due to the nature of 2 PA materials that possess deep florescence penetration in biological tissue. In conclusion, the complex **1** displays much lower toxicity and brighter two-photon fluorescent bioimaging than its free ligand, which make it successfully applied to a two-photon fluorescent probe for detecting the cytoplasm section in HepG2 cells.

4. Conclusions

A series of thiocyanate complexes incorporating a functional chromophore to get a two-photon enhanced effect by crystal engineering were synthesized. In the spectral region of interest (700–900 nm), the functionalized complexes 1–6 exhibit much larger 2 PA cross-section values, higher quantum yield and thermal stability compared to the free chromophore. The hetero-metal complexes have greater 2 PA cross-section values than those of homo-nuclear metal ions complexes. The results exhibit that the transition metal ions serve as multidimensional templates to control the crystal structures, and further tailor the fluorescence quantum yields and 2 PA cross-sections. In addition, two-photon fluorescence cell imaging experiment results showed that complex 1 is clearly capable of detecting the cytoplasm section in HepG2 cells. These results emphasize the high potentialities of this class of complexes: combining the advantage of both transition metal ions with two-photon microscopy biological imaging application recently was demonstrated, which opened the way to an improved biological imaging technique.

Acknowledgments

This work was supported by a grant for the National Natural Science Foundation of China (21271004, 51372003, 51432001, and 21271003), the Natural Science Foundation of Anhui Province (1208085MB22, 1308085MB24), Ministry of Education Funded Projects Focus on returned overseas scholar. Program for New Century Excellent Talents in University (China) and Doctoral Program Foundation of Ministry of Education of China (20113401110004).

Appendix A. Supplementary data

Supplementary data related to this article can be found at http://dx.doi.org/10.1016/j.dyepig.2015.03.039.

References

[1] Hu MY, Li L, Wu H, Su Y, Yang PY, Uttamchandani M, et al. Multicolor, one- and two-photon imaging of enzymatic activities in live cells with fluorescently quenched activity-based probes (qABPs). J Am Chem Soc 2011;133:12009–20.
[2] Zhang CJ, Li L, Chen GYJ, Xu QH, Yao SQ. One- and two-photon live cell imaging using a mutant SNAP-tag protein and its FRET substrate pairs. Org Lett 2011;13:4160–3.
[3] Sumalekshmy S, Henary MM, Siegel N, Lawson PV, Wu Y, Schmidt K, et al. Design of emission ratiometric metal-ion sensors with enhanced two-photon cross section and brightness. J Am Chem Soc 2007;129:11888–9.
[4] He GS, Tan LS, Zheng Q, Prasad PN. Multiphoton absorbing materials: molecular designs, characterizations, and applications. Chem Rev 2008;108:1245–330.
[5] Zhang XJ, Ren XS, Xu QH, Loh KP, Chen ZK. One- and two-photon turn-on fluorescent probe for cysteine and homocysteine with large emission shift. Org Lett 2009;11:1257–60.
[6] Pawlicki M, Collins HA, Denning RG, Anderson HL. Two-photon absorption and the design of two-photon dyes. Angew Chem Int Ed 2009;48:3244–66.
[7] Cepraga C, Gallavardin T, Marotte S, Lanoe PH, Mulatier JC, Lerouge F, et al. Biocompatible well-defined chromophore-polymer conjugates for photodynamic therapy and two-photon imaging. Poly Chem 2013;4:61–7.
[8] Geng JL, Goh CC, Tomczak N, Liu J, Liu RR, Ma L, et al. Micelle/Silica co-protected conjugated polymer nanoparticles for two-photon excited brain vascular imaging. Chem Mater 2014;26:1874–80.
[9] LaFratta CN, Fourkas JT, Baldacchini T, Farrer RA. Multiphoton fabrication. Angew Chem Int Ed 2007;46:6238–58.
[10] Nazir R, Danilevicius P, Ciuciu AI, Chatzinikolaidou M, Gray D, Flamigni L, et al. π-Expanded ketocoumarins as efficient, biocompatible initiators for two-photon-induced polymerization. Chem Mater 2014;26:3175–84.
[11] Sivakumar S, van Veggel F, May PS. Near-infrared (NIR) to red and green up-conversion emission from silica sol-gel thin films made with $La_{0.45}Yb_{0.50}Er_{0.05}F_3$ nanoparticles, hetero-looping-enhanced energy transfer (Hetero-LEET): a new up-conversion process. J Am Chem Soc 2007;129:620–5.
[12] Zhang X, Yang PAP, Wang D, Xu J, Li CX, Gai SL, et al. $La(OH)_{(3)}:Ln^{(3+)}$ and $La_2O_3:Ln^{(3+)}$ (Ln = Yb/Er, Yb/Tm, Yb/Ho) microrods: synthesis and up-conversion luminescence properties. Cryst Growth Des 2012;12:306–12.
[13] Markowicz PP, He GS, Prasad PN. Direct four-photon excitation of amplified spontaneous emission in a nonlinear organic chromophore. Opt Lett 2005;30:1369–71.
[14] Fan HH, Wang HZ, Tian YP. Four-photon process induced upconversion lasing. Chin Phys Lett 2005;22:1152–4.
[15] Chen GY, Qju HL, Prasad PN, Chen XY. Upconversion nanoparticles: design, nanochemistry, and applications in theranostics. Chem Rev 2014;114:5161–214.
[16] Ramakrishna G, Varnavski O, Kim J, Lee D, Goodson T. Quantum-sized gold clusters as efficient two-photon absorbers. J Am Chem Soc 2008;130:5032–3.
[17] He GS, Zheng QD, Prasad PN, Helgeson R, Wudl F. Nonlinear optical stabilization of 1064-nm laser pulses with a two-photon absorbing liquid-dye salt system. Appl Opt 2005;44:3560–4.
[18] Glimsdal E, Carlsson M, Kindahl T, Lindgren M, Lopes C, Eliasson B. Luminescence, singlet oxygen production, and optical power limiting of some diacetylide Platinum(II) diphosphine complexes. J Phys Chem A 2010;114:3431–42.
[19] Robinson JT, Hong GS, Liang YY, Zhang B, Yaghi OK, Dai HJ. In vivo fluorescence imaging in the second near-infrared window with long circulating carbon nanotubes capable of ultrahigh tumor uptake. J Am Chem Soc 2012;134:10664–9.
[20] Wang XH, Morales AR, Urakami T, Zhang LF, Bondar MV, Komatsu M, et al. Folate receptor-targeted aggregation-enhanced near-IR emitting silica

nanoprobe for one-photon in vivo and two-photon ex vivo fluorescence bioimaging. Bioconjugate Chem 2011;22:1438–50.
[21] Ishow E, Brosseau A, Clavier G, Nakatani K, Pansu RB, Vachon JJ, et al. Two-photon fluorescent holographic rewritable micropatterning. J Am Chem Soc 2007;129:8970–1.
[22] Luchita G, Bondar MV, Yao S, Mikhailov IA, Yanez CO, Przhonska OV, et al. Efficient photochromic transformation of a new fluorenyl diarylethene: one- and two-photon absorption spectroscopy. ACS Appl Mater Interfaces 2011;3:3559–67.
[23] Tian YP, Li L, Zhang JZ, Yang JX, Zhou HP, Wu JY, et al. Investigations and facile synthesis of a series of novel multi-functional two-photon absorption materials. J Mater Chem 2007;17:3646–54.
[24] Jiang GY, Wang S, Yuan WF, Jiang L, Song YL, Tian H, et al. Highly fluorescent contrast for rewritable optical storage based on photochromic bisthienylethene-bridged naphthalimide dimer. Chem Mater 2006;18:235–7.
[25] Jhaveri SJ, McMullen JD, Sijbesma R, Tan LS, Zipfel W, Ober CK. Direct three-dimensional microfabrication of hydrogels via two-photon lithography in aqueous solution. Chem Mater 2009;21:2003–6.
[26] Yuan HX, Chong H, Wang B, Zhu CL, Liu LB, Yang Q, et al. Chemical molecule-induced light-activated system for anticancer and antifungal activities. J Am Chem Soc 2012;134:13184–7.
[27] Hammerer F, Garcia G, Chen S, Poyer F, Achelle S, Fiorini-Debuisschert C, et al. Synthesis and characterization of glycoconjugated porphyrin triphenylamine hybrids for targeted two-photon photodynamic therapy. J Org Chem 2014;79:1406–17.
[28] Lee JH, Lim CS, Tian YS, Han JH, Cho BR. A two-photon fluorescent probe for thiols in live cells and tissues. J Am Chem Soc 2010;132:1216–7.
[29] Rao AS, Kim D, Wang T, Kim KH, Hwang S, Ahn KH. Reaction-Based two-photon probes for mercury ions: fluorescence imaging with dual optical windows. Org Lett 2012;14:2598–601.
[30] Kang DE, Lim CS, Kim JY, Kim ES, Chun HJ, Cho BR. Two-photon probe for Cu^{2+} with an internal reference: quantitative estimation of Cu^{2+} in human tissues by two-photon microscopy. Anal Chem 2014;86:5353–9.
[31] Alam MM, Chattopadhyaya M, Chakrabarti S, Ruud K. Chemical control of channel interference in two-photon absorption processes. Acc Chem Res 2014;47:1604–12.
[32] Jiang YH, Wang YC, Hua JL, Tang J, Li B, Qian SX, et al. Multibranched triarylamine end-capped triazines with aggregation-induced emission and large two-photon absorption cross-sections. Chem Commun 2010;46:4689–91.
[33] Huang W, Wang H, Sun L, Li B, Su JH, Tian H. Propeller-like D–π–A architectures: bright solid emitters with AIEE activity and large two-photon absorption. J Mater Chem C 2014;2:6843–9.
[34] Dichtel WR, Serin JM, Edder C, Frechet JMJ, Matuszewski M, Tan LS, et al. Singlet oxygen generation via two-photon excited FRET. J Am Chem Soc 2004;126:5380–1.
[35] D'Aleo A, Picot A, Baldeck PL, Andraud C, Maury O. Design of dipicolinic acid ligands for the two-photon sensitized luminescence of europium complexes with optimized cross-sections. Inorg Chem 2008;47:10269–79.
[36] Das S, Nag A, Goswami D, Bharadwaj PK. Zinc(II)- and copper(I)-mediated large two-photon absorption cross sections in a bis-cinnamaldiminato Schiff base. J Am Chem Soc 2006;128:402–3.
[37] Drobizhev M, Stepanenko Y, Dzenis Y, Karotki A, Rebane A, Taylor PN, et al. Understanding strong two-photon absorption in pi-conjugated porphyrin dimers via double-resonance enhancement in a three-level model. J Am Chem Soc 2004;126:15352–3.
[38] Rendon N, Bourdolle A, Baldeck PL, Le Bozec H, Andraud C, Brasselet S, et al. Bright luminescent silica nanoparticles for two-photon microscopy imaging via controlled formation of 4,4'-diethylaminostyryl-2,2'-bipyridine Zn(II) surface complexes. Chem Mater 2011;23:3228–36.
[39] Zhang ML, Tian YP, Zhang XJ, Wu JY, Zhang SY, Wang D, et al. Synthesis, crystal structure and two-photon property studies on a series of complexes derived from a novel Schiff base ligand. Transit Met Chem 2004;29:596–602.
[40] Zhang XJ, Tian YP, Jin F, Wu JY, Xie Y, Tao XT, et al. Self-assembly of an organic chromophore with Cd-s nanoclusters: supramolecular structures and enhanced emissions. Cryst Growth Des 2005;5:565–70.
[41] Zhou HP, Li DM, Zhang JZ, Zhu YM, Wu JY, Hu ZJ, et al. Crystal structures, optical properties and theoretical calculation of novel two-photon polymerization initiators. Chem Phys 2006;322:459–70.
[42] Hou HW, Wei YL, Song YL, Mi LW, Tang MS, Li LK, et al. Metal ions play different roles in the third-order nonlinear optical properties of $d(^{10})$ metal-organic clusters. Angew Chem Int Ed 2005;44:6067–74.
[43] Xu H, Song YL, Mi LW, Hou HW, Tang MS, Sang YL, et al. Coordination frameworks constructed from bipyridyl piperazine and MCl_2 (M = Co, Ni, Zn): structural characterization and optical properties. Dalton Trans 2006:838–45.
[44] Wang XC, Tian XH, Zhang Q, Sun PP, Wu JY, Zhou HP, et al. Assembly, two-photon absorption, and bioimaging of living cells of A cuprous cluster. Chem Mater 2012;24:954–61.
[45] Drobizhev M, Stepanenko Y, Rebane A, Wilson CJ, Screen TEO, Anderson HL. Strong cooperative enhancement of two-photon absorption in double-strand conjugated porphyrin ladder arrays. J Am Chem Soc 2006;128:12432–3.
[46] Samoc M, Morrall JP, Dalton GT, Cifuentes MP, Humphrey MG. Two-photon and three-photon absorption in an organometallic dendrimer. Angew Chem Int Ed 2007;46:731–3.
[47] Righetto S, Rondena S, Locatelli D, Roberto D, Tessore F, Ugo R, et al. An investigation on the two-photon absorption activity of various terpyridines and related homoleptic and heteroleptic cationic Zn(II) complexes. J Mater Chem 2006;16:1439–44.
[48] Picot A, Malvolti F, Le Guennic B, Baldeck PL, Williams JAG, Andraud C, et al. Two-photon antenna effect induced in octupolar europium complexes. Inorg Chem 2007;46:2659–65.
[49] Wang J, Sun ZR, Deng L, Wei ZH, Zhang WH, Zhang Y, et al. Reactions of a tungsten trisulfido complex of hydridotris(3,5-dimethylpyrazol-1-yl)borate (Tp^*) $[Et_4N][Tp^*WS_3]$ with CuX (X = Cl, NCS, or CN): isolation, structures, and third-order NLO properties. Inorg Chem 2007;46:11381–9.
[50] Liu HJ, Tao XT, Yang JX, Yan YX, Ren Y, Zhao HP, et al. Three-dimensional metal-organic network architecture with large pi-conjugated indolocarbazole derivative: synthesis, supramolecular structure, and highly enhanced fluorescence. Cryst Growth Des 2008;8:259–64.
[51] Li SL, Wu JY, Tian YP, Ming H, Wang P, Jiang MH, et al. Design, crystal growth, characterization, and second-order nonlinear optical properties of two new three-dimensional coordination polymers containing selenocyanate ligands. Eur J Inorg Chem 2006:2900–7.
[52] Tancrez N, Feuvrie C, Ledoux I, Zyss J, Toupet L, Le Bozec H, et al. Lanthanide complexes for second order nonlinear optics: evidence for the direct contribution of f electrons to the quadratic hyperpolarizability. J Am Chem Soc 2005;127:13474–5.
[53] Eagle AA, Gable RW, Thomas S, Sproules SA, Young CG. Sulfur atom transfer reactions of tungsten(VI) and tungsten(IV) chalcogenide complexes. Polyhedron 2004;23:385–94.
[54] Doonan CJ, Nielsen DJ, Smith PD, White JM, George GN, Young CG. Models for the molybdenum hydroxylases: synthesis, characterization and reactivity of cis-oxosulfido-Mo(VI) complexes. J Am Chem Soc 2006;128:305–16.
[55] Sheldrick GM. SHELXL-97. Program for crystal structures refinement. University of; 1997.
[56] Van Albada GA, De Graaff RAG, Jhaasnoot AG, Reedijk J. Synthesis, spectroscopic characterization, and magnetic properties of unusual 3,5-dialkyl- 1,2,4-triazole compounds containing N-bridging isothiocyanato ligands. X-ray structure of trinuclear Bis[(p-thiocyanato-N)bis(p-3,5-diethyl-1,2,4-t riazole-N1,N2)bis(tbiocyanato-N)(3,5-diethyl-1,2,4-triazole-N1)nickel(II)-N,N1,N1'] nickel(II) dihydrate. Inorg Chem 1984;23:1404–8.
[57] Ren Y, Yu XQ, Zhang DJ, Wang D, Zhang ML, Xu GB, et al. Synthesis, structure and properties of a new two-photon photopolymerization initiator. J Mater Chem 2002;12:3431–7.
[58] Zhang HW, Ximin, Teo Boon K. Molecular design and crystal engineering of a new series of inorganic polymers separated by organic spacers: structures of $[(18C6)K][Cd(SCN)_3]$ and $[(18C6)_2Na_2(H_2O)_2]1/2[Cd(SCN)_3]$. J Am Chem Soc 1996;118:11813–21.
[59] Hou H, Meng X, Song Y, Fan Y, Zhu Y, Lu H, et al. Two-dimensional rhombohedral grid coordination polymers $[M(bbbt)_2(NCS)_2]n$(M = Co, Mn, or Cd; bbbt = 1,1'-(1,4-butanediyl) bis-1H-benzotriazole): synthesis, crystal structures, and third-order nonlinear optical properties. Inorg Chem 2002;41:4068–75.
[60] Horikoshi R, Nambu C, Mochida T. Metal-centered ferrocene clusters from 5-ferrocenylpyrimidine and ferrocenylpyrazine. Inorg Chem 2003;42:6868–75.
[61] Yi L, Ding B, Zhao B, Cheng P, Liao DZ, Yan SP, et al. Novel triazole-bridged cadmium coordination polymers varying from zero-to three-dimensionality. Inorg Chem 2004;43:33–43.
[62] Batten SRR, Richard. Interpenetrating nets: ordered, periodic entanglement. Angew Chem Int Ed 1998;37:1460–94.
[63] Zheng QD, He GS, Prasad PN. Novel two-photon-absorbing, 1,10-phenanthroline-containing pi-conjugated chromophores and their nickel(II) chelated complexes with quenched emissions. J Mater Chem 2005;15:579–87.
[64] Mongin O, Porres L, Charlot M, Katan C, Blanchard-Desce M. Synthesis, fluorescence, and two-photon absorption of a series of elongated rodlike and banana-shaped quadrupolar fluorophores: a comprehensive study of structure–property relationships. Chem Eur J 2007;13:1481–98.
[65] Han H, Song YL, Hou HW, Fan YT, Zhu Y. A series of metal-organic polymers assembled from MCl_2 (M = Zn, Cd, Co, Cu): structures, third-order nonlinear optical and fluorescent properties. Dalton Trans 2006:1972–80.
[66] Niu YY, Song YL, Hou HW, Zhu Y. Synthesis, structure, and large optical limiting effect of the first coordination polymeric cluster based on an {I@AgI(inh) (6)} hexagram block. Inorg Chem 2005;44:2553–9.
[67] Siemeling U, Rother D, Bruhn C, Fink H, Weidner T, Trager F, et al. The interaction of 1,1 '-diisocyanoferrocene with gold: formation of monolayers and supramolecular polymerization of an aurophilic ferrocenophane. J Am Chem Soc 2005;127:1102–3.
[68] Zhang X, Xie Y, Zhao Q, Tian Y. 1-D coordination polymer template approach to CdS and HgS aligned-nanowire bundles. New J Chem 2003;27:827–30.
[69] Hao FY, Zhang XJ, Tian YP, Zhou HP, Li L, Wu JY, et al. Design, crystal structures and enhanced frequency-upconverted lasing efficiencies of a new series of dyes from hybrid of inorganic polymers and organic chromophores. J Mater Chem 2009;19:9163–9.